# ANALYSIS OF CUMULUS SOLAR IRRADIANCE REFLECTANCE (CSIR) EVENTS

John L. Laird and Harshvardhan*

Department of Earth & Atmospheric Sciences

Purdue University

West Lafayette, IN 47907

*to whom correspondence should be addressed.
e-mail: harsh@summer.atms.purdue.edu
fax: 1-317-496-1210

**Abstract**

Clouds are extremely important with regard to the transfer of solar radiation at the earth's surface. This study investigates Cumulus Solar Irradiance Reflection (CSIR) using ground-based pyranometers. CSIR events are short-term increases in solar radiation observed at the surface as a result of reflection off the sides of convective clouds. When sun-cloud observer geometry is favorable, these occurrences produce characteristic spikes in the pyranometer traces and solar irradiance values may exceed expected clear-sky values. Ultraviolet CSIR events were investigated during the summer of 1995 using Yankee Environmental Systems UVA-1 and UVB-1 pyranometers. Observed data were compared to clear-sky curves which were generated using a third degree polynomial best-fit line technique. Periods during which the observed data exceeded this clear-sky curve were identified as CSIR events. The magnitude of a CSIR event was determined by two different quantitative calculations. The MAC (magnitude above clear-sky) is an absolute measure of the difference between the observed and clear-sky irradiances. Maximum MAC values of 3.4 $Wm^{-2}$ and 0.069 $Wm^{-2}$ were observed at the UV-A and UV-B wavelengths, respectively. The second calculation determined the percentage above clear-sky (PAC) which indicated the relative magnitude of a CSIR event. Maximum UV-A and UV-B PAC magnitudes of 10.1% and 7.8%, respectively, were observed during the study. Also of interest was the duration of the CSIR events which is a function of sun-cloud-sensor geometry and the speed of cloud propagation over the measuring site. In both the UV-A and UV-B wavelengths, significant CSIR durations of up to 30 minutes were observed.

## 1. Introduction

Currently, there is a great deal of interest in the shortwave radiation budget of the atmosphere. Whereas satellite measurements have provided very narrow bounds on the total solar absorption by the earth-atmosphere system, the partition of this absorbed energy between the surface and the atmosphere is determined by differencing shortwave measurements at the boundaries of an atmospheric column. Obtaining this residual accurately is an extremely difficult task and recent attempts have yielded values that are at variance with theoretical estimates based on the optical properties of the clear and cloudy atmosphere (Cess et al., 1995; Ramanathan et al., 1995; Pilewskie and Valero, 1995).

One difficulty with interpreting solar transmission measurements is the large excursion in the value of the transmitted irradiance when the sky is partly cloudy and there is reflection off cloud sides into the fields of view of the measuring instrument. This phenomenon has been termed Cumulus Solar Irradiance Reflection (CSIR) by Segal and Davis (1992) and in many cases, the irradiance exceeds the corresponding clear-sky values for the same time of day. CSIR events are usually short in duration, lasting up to an hour depending on cloud height, orientation of the sun, and prevailing wind speed.

Previous studies specifically designed to examine CSIR events are few in number. Segal and Davis (1992) have conducted research of CSIR events with regard to total shortwave flux, while Mims and Frederick (1994) have documented CSIR in UV-B traces during the Hawaii Ultraviolet Survey. A Japanese effort by Hayasaka et al. (1995) used aircraft to report the fluxes above and below stratocumulus clouds. In the vicinity of the cloud wall, downward flux below the cloud was larger than the downward flux above the cloud (i.e. clear-sky), indicating a CSIR event. In all cases, irradiance measurements showed an increase over the expected clear-sky values. While each of the aforementioned studies has CSIR in common, their differences lie in the magnitudes (% above clear-sky values) of these events. In the Segal and Davis (1992) work, peak shortwave enhancement was approximately 30%, while in Mims and Frederick (1994) the UV-B flux exhibited a 29% peak increase at the surface in Hawaii. Japanese measurements

showed increases on the order of a few percent (Hayasaka et al., 1995). From these results, it is unclear if the large variation in CSIR enhancement is due to the differences in site location, sun orientation, or atmospheric conditions.

Numerical models have also shown significant effects from cloud-side reflection. However, large scale climate models use the plane-parallel approximation to represent the atmosphere. This approximation assumes clouds to be flat plates with infinite or semi-infinite horizontal extent. CSIR events occur during fractional cloud cover and involve reflection off of clouds with significant vertical dimensions. Errors are introduced into the plane-parallel approximation in situations where the cloud sides are illuminated by direct and diffuse radiation (McKee and Cox, 1974; Davies, 1978; Weinman and Harshvardhan, 1982; Harshvardhan and Thomas, 1984). As a result, various computational methods have been developed to incorporate finite cloud schemes into these models to allow for the occurrence of cloud-side reflection. Some examples of these schemes are described in Nack and Green (1974) or Harshvardhan and Thomas (1984). Using these various finite cloud schemes, CSIR has been validated by computational models. Nack and Green (1974) predicted CSIR events in the middle ultraviolet spectrum, while Cahalan et al. (1994) showed significant increases in downward flux compared to the plane-parallel model as a result of reflection off of illuminated cloud sites. Segal and Davis (1992) and Hayasaka et al. (1995) used model data as a comparison tool with their measurements. These model results also incorporated information on the horizontal extent of CSIR from the boundary of the cloud. CSIR effects diminished with distance from the cloud/clear-sky boundary but varied as a function of cloud height and zenith angle.

The impact of CSIR events on the daily shortwave receipt is not climatologically significant for normal continental locations. Random cloudiness creates significant shadowing effects which dominate the daily integrated total. As expected, this total is less than the total for a clear-sky situation on the same day. However, the short term increases in solar radiation could still be considered important in regions with nonrandom cloudiness. Nonrandom cloudiness is a repetitive feature in terms of time of day, location, and season and is usually a result of terrain-

induced thermal circulations (Weaver and Segal, 1988). In these cases, Segal and Davis (1992) suggest that CSIR may impact surface visibility, the dissipation of morning inversions, and plant photosynthesis. Also, serious biological effects are possible with increased UV-B amounts at the surface as a result of cloud side reflection (Mims and Frederick, 1994).

The purpose of this study was to compare the magnitudes of CSIR events in the shortwave, UV-A, and UV-B wavelength ranges for a typical midlatitude location. The measured irradiance data were compared to the clear-sky trace in order to determine the magnitudes of the CSIR events for the wavelength ranges in question. Ratios of observed irradiance to clear-sky irradiance were calculated for each radiative parameter to provide a common basis for comparison. CSIR events were denoted by ratios which had magnitudes larger than one. These ratios were then compared with the hope of determining differences or similarities in the magnitude of CSIR events in each of the solar spectral ranges.

## 2. Instrumentation

Measurements were taken from the Purdue Rooftop Atmospheric Measurement Facility (RARMF). This site has coordinates of 40.43 °N latitude and 86.92 °W longitude. The instrument platform is located 210 meters above mean sea level. The RARMF rooftop supports a variety of instruments. Of relevance here are the Weathertronics SW Pyranometer, Yankee Environmental Systems UVA-1 and UVB-1 pyranometers and Vaisala laser ceilometer. Ultraviolet CSIR events were investigated during the summer of 1995 using the Y.E.S. pyranometers. The instruments use colored glass filters and UV-A and UV-B (depending on the instrument) sensitive phosphors to block portions of the solar spectrum not within the specified wavelength range. The phosphor is then converted to visible (green) light where it is measured by a solid state photodetector. The effective (measured) ultraviolet irradiance measured by either pyranometer is a result of the convolution of the ultraviolet spectral distribution and the pyranometer spectral response (Y.E.S. UVA-1 Operations Manual, 1991; Y.E.S. UVB-1 Operations Manual, 1991).

Three different methods of absolute calibration were conducted by the manufacturer to ensure accurate performance of the pyranometers. A spectral calibration was performed with a Xenon arc lamp and a reference detector. Also, the sensors were placed outdoors and calibrated with a standard UV pyranometer. Finally, the pyranometer output was compared to the calculated UV values on a clear day, near solar noon. The Y.E.S. UVA-1 pyranometer is designed with a spectral response of 320 to 400 nanometers and a sensitivity of 0.063 Volts/$Wm^{-2}$ of effective UV-A irradiance. The cosine response is $\pm 1\%$ for zenith angles between 0°-30° and $\pm 5\%$ for angles between 0°-60° (Y.E.S. UVA-1 Operations Manual, 1991). The specifications of the Y.E.S. UVB-1 pyranometer are quite different than that of the UVA-1 instrument. The spectral response ranges from 280 to 330 nanometers, however, the conversion factors used in processing the raw data reduced the effective wavelength interval to the standard UV-B range from 280 to 320 nanometers (Y.E.S. UVB-1 Operations Manual, 1991). The sensitivity of the UVB-1 pyranometer is highly dependent on zenith angle, unlike the UVA-1 instrument and conversion factors were applied for the particular zenith angle (Y.E.S. UVB-1 Technical Note 93-01).

Under operating conditions, it was discovered that during the nighttime hours the irradiance measurements varied significantly from zero. The nighttime pattern of error correlated well with the diurnal temperature pattern. A temperature correction was therefore applied, using the Purdue University Airport temperature measurements since temperature was not recorded at the rooftop site. This ambient temperature correction was subsequently used for all CSIR data.

## 3. CSIR Methodology

The enhancement effects of a CSIR event are highly variable and may or may not significantly increase surface irradiance. However, with the proper sun-cloud sensor geometry, cloud-side reflection will increase total global flux above clear-sky values. For a ground-based measurement system, the pyranometer will be illuminated by the direct component of the sun's radiation during a CSIR event. In addition, there will be some diffuse radiation from a cloud side impinging on the instrument. The increase in radiation measured at the surface as a result of

CSIR is dependent on the amount of diffuse radiation scattered into the solid angle subtended by the projection of the cloud-side area normal to the sensor.

There are many factors which affect the magnitude of the CSIR radiation enhancement. Through model simulations, Segal and Davis (1992) suggested that the magnitude of cloud reflection events increases with increasing cloud height and decreasing zenith angle. This is reasonable since the larger the area of the illuminated cloud side, the larger the normal projection relative to the pyranometer. This, in turn, will increase the solid angle encompassing the diffuse radiation scattered from the cloud. Also, increasing the zenith angle increases the effective cloud fraction due to cloud geometry, as discussed by Harshvardhan and Thomas (1984). At some critical zenith angle, cloud elements will begin to shadow one another, cutting off the surface from any direct component of solar radiation and eliminating the possibility of CSIR events. Other factors affecting CSIR magnitude include cloud optical depth, atmospheric aerosol concentration, and atmospheric column ozone.

The first step in the investigation of cloud-side reflection events was to determine likely days on which this phenomenon may occur. June, July, and August 1995 were inspected for possible CSIR for several reasons. Higher zenith angles provided for more favorable reflection geometry and reduced the possibility of shadowing effects from adjacent clouds. Summer months also have high solar irradiance values at the surface, which made for more pronounced CSIR events. The most pronounced vertical cloud development, and therefore larger CSIR magnitudes, was expected during the summer months due to favorable dynamic forcing processes and higher amounts of atmospheric water vapor.

Four different criteria were used in determining if a particular day exhibited CSIR events.

1. Significant positive spikes above clear-sky values existed in the RARMF pyranometer data.
2. Scattered cloud conditions were reported in the vicinity of the RARMF.
3. Clouds passed over the RARMF.
4. No haze was reported in conjunction with the scattered clouds.

These criteria were verified by the inspection of the daily pyranometer data, hourly surface observations from the Purdue University Airport and half-hourly visible GOES satellite images.

The most crucial part in the investigation of CSIR events, other than ensuring the accuracy of the measurements, was the development of the clear-sky curves with which the observed data could be compared. In previous studies (Segal and Davis, 1992; Mims and Frederick, 1994), observed pyranometer data were used from a clear-sky day adjacent to the exhibiting CSIR events. However, clear-sky days are rare over West Lafayette due to the summertime synoptic conditions typical of mid-latitude locales. This being the case, a modified method from Frederick and Snell (1990) was used to generate the clear-sky curves. Frederick and Snell composed clear-sky traces for climatological purposes using half-hourly averages of ultraviolet irradiance over the span of a month. Then for a fixed time, each day of the month was compared and the largest irradiance value was selected. These maxima were deemed the clear-sky values for the month and composited into a single curve.

Using this basic concept, clear-sky curves were created for the shortwave, UV-A, and UV-B wavelength ranges corresponding to each of the seven days selected for this study. The accuracy of the traces was crucial because it would greatly affect the calculation of the CSIR magnitudes. However, instead of generating curves using an entire month of data, two or three select days were used. Table 1 lists the CSIR days chosen for this study and the days used to create the corresponding clear-sky curves. It should be noted that a number of the CSIR days were used in the composite process as they provided a substantial contribution to their own corresponding clear-sky traces.

Instead of the half-hour averages used by Frederick and Snell (1990), RARMF instrument data was averaged over 10 minute intervals. The days used in the composite were chosen because either part of the day provided clear-sky conditions or the variability in irradiance caused by scattered cloud conditions would be smoothed in the averaging process. The corresponding 10 minute bins from each day were then compared and the largest values were selected for the clear-sky curve. Using the maximum values did create a problem in instances where the actual

CSIR day was used in the compositing process. In these cases, the 10 minute averages did not totally eliminate the CSIR events found in the pyranometer data. Therefore, some of the maximum values were larger than the expected clear-sky trace. Negative spikes also appeared in the composite curves if cloudiness was present at the same time for each day. Figure 1 shows an example of a clear-sky trace generated from three days in August, 1995. The problems of lingering CSIR effects and cloud related underestimation are clearly evident between 14 and 16 EST. The major drawback with using the composite technique is that the time-averages of real data do not produce a smooth clear-sky curve necessary for the analysis of CSIR magnitudes.

In order to correct for this smoothness problem, the composite trace was further processed using best-fit curve techniques. It was possible to eliminate spikes in the clear-sky curves by fitting a best-fit line to the averaged irradiance data. However attempting this for data in the form of Fig. 1 (irradiance vs. time) would still produce an asymmetrical and potentially non-smooth trace. As a result, irradiance measurements were plotted versus the cosine of the zenith angle as shown by Fig. 2. Also illustrated in the figure is the third degree polynomial best-fit line corresponding to the plotted data. This best-fit line procedure was applied to the shortwave, UV-A, and UV-B data on all seven CSIR days and related clear-sky irradiance to the cosine of the zenith angle. Zenith angles averaged over 2 minutes were used in the best-fit line equations to generate the corresponding clear-sky irradiances. The resulting curves were then used in the final comparison with the observed data. Fig. 3 shows the curve from Fig. 1 superimposed with final clear-sky trace generated from the best-fit line technique. The next step in the study was the evaluation of the CSIR magnitudes.

## 4. CSIR Events

The analysis of the CSIR phenomenon was conducted by comparing observed RARMF data with the generated clear-sky curves. Seven days, listed in Table 1, from the summer of 1995 exhibited cloud reflection characteristics of CSIR and were analyzed in this study. Inspection of GOES visible satellite images showed the regional extent of the clouds which affected the West Lafayette area at a selected time during which CSIR events occurred. With the exception of July

3, scattered fair weather cumulus clouds were present in the vicinity of the RARMF during the CSIR events. On July 3, a cirrus deck covered the area but surface observations indicated lightly scattered clouds at low altitudes.

The RARMF Vaisala laser ceilometer provided a more localized source to determine if clouds were present over the West Lafayette area, and the RARMF in particular. The determination of cloud base height for scattered clouds proved to be inaccurate so the ceilometer was only used to detect the passage of clouds over the RARMF which could have produced the CSIR events recorded by the RARMF pyranometers. Figure 4 shows the ceilometer trace for July 18. The ceilometer data for each day was compared with the shortwave pyranometer traces from the corresponding day. In general, there was good temporal correlation between the cloud data and the occurrence of shortwave CSIR.

*4.1 Results*

CSIR events occurred when the observed RARMF fluxes in the total shortwave, UV-A and UV-B wavelength ranges exceeded the expected surface values at a specific time of day. Figure 5, 6 and 7 show the shortwave, UV-A and UV-B irradiances, respectively for July 18 and clear-sky irradiances generated by the technique mentioned previously. Other days also showed CSIR phenomena to varying degrees.

The most obvious feature seen when comparing the plots between the different wavelength ranges for each day is that the relative magnitudes of the total shortwave CSIR events are markedly larger than those observed in the UV-A and UV-B wavelengths. This result was to be expected due to the diffuse nature of the radiation at the ultraviolet wavelengths. UV-A and UV-B radiation is scattered much more efficiently by atmospheric aerosols and air molecules compared to the entire shortwave spectrum. This being the case, the cloud side is not illuminated as strongly by the direct component of the ultraviolet irradiance. The reduction in irradiance from the direct sun-sensor path also reduces the amount of radiation preferentially scattered towards the pyranometer by the cloud resulting in reduced CSIR magnitudes. An extreme

example on August 15 (not shown) showed pronounced CSIR events occurring in the total shortwave but appearing only minimally in the UV-A and were absent in the UV-B wavelengths.

In every case except for July 18, all significant CSIR activity occurred at solar noon, which is approximately 12:58 EST for West Lafayette, or during the afternoon hours. This can be linked to the summertime sky conditions which most likely evolved in a similar manner on all seven days. The mornings were generally clear allowing for the receipt of the maximum amount of solar radiation at the surface. As is typical in mid-latitude summers, this induces convective activity which results in scattered cumulus conditions throughout the rest of the day.

*4.2 MAC and PAC Calculations*

The CSIR events can be depicted quantitatively using two measures — magnitude above clear-sky (MAC) and percentage above clear-sky irradiance (PAC). Positive values of MAC and PAC correspond to CSIR events; PAC allows a comparison of CSIR events between different wavelengths. Figures 8, 9 and 10 show MAC and PAC for the three wavelength intervals for July 18, corresponding to Figures 5, 6, and 7. As mentioned earlier, the clear-sky traces were generated using a third degree polynomial best-fit line. The clear-sky curve did not approximate the observed irradiances well at low sun angles and this systematic discrepancy is apparent in all MAC traces. The error appears as two artificial CSIR events near sunrise and sunset. Since the absolute magnitude of the irradiance is small, these errors can be ignored. In order not to swamp the PAC curves with these spurious data, PAC values in excess of 50% are not plotted. This threshold was large enough to include all daytime CSIR events. Table 2 lists the maximum MAC values for each of the CSIR days and each of the wavelength ranges studied. The PAC values are not the maximum values observed for that day but are the magnitudes which are associated with the maximum MAC events in the adjacent column. It should also be noted that the maximum MAC values in each wavelength range are independent of one another and do not necessarily correspond to the same CSIR event.

All MAC and PAC calculations correspond to the observed RARMF data averaged over 2 minutes. However, larger MAC and PAC values would be expected using the instantaneous

data. The largest shortwave MAC occurred on July 18 with a value of 151.5 $Wm^{-2}$ and a corresponding PAC of 16.6%. Recall that Segal and Davis (1992) performed their study on the shortwave spectrum, and while they did not publish quantitative statistics, they estimated their largest MAC at 250 $Wm^{-2}$ with a PAC of approximately 30%.

In general, the MAC and PAC values encountered by Segal and Davis (1992) were expected to exceed those generated using the RARMF data. Segal and Davis conducted their study in Colorado under the influence of deep convective clouds, in contrast to the fair weather cumulus encountered over West Lafayette in this study. One of the most important factors in determining the magnitude of CSIR events is cloud size. While the exact sun-cloud-sensor geometry was not known in this or the Colorado study, the large differences in MAC values were most likely due to the significant difference in cloud conditions.

The largest total shortwave PAC value was observed on July 18 at 16.6%. The significance of the PAC calculation is to determine the relative intensity of a CSIR event. Because the PAC is a ratio, the larger PAC values were not necessarily found near solar noon and could be expected throughout the day. This is contrary to the maximum MAC values, which were mostly observed around midday, the time of maximum insolation. For the most part, however, the larger shortwave PAC values did correspond closely with the larger shortwave MAC events.

The ultraviolet wavelengths, while exhibiting the effects of CSIR, showed greatly reduced MAC and PAC values compared to the shortwave. The maximum observed PAC magnitudes were 10.1% and 7.8% for the UV-A and UV-B, respectively. Mims and Frederick (1994) observed a peak PAC of 29% around solar noon which is substantially larger than the maximum value recorded from the RARMF. The Mauna Loa Observatory, Hawaii, where Mims and Frederick observed this UV-B PAC value, is located 3.4 kilometers above sea level. At this height, the air column density is much less than the corresponding value encountered in West Lafayette. Air molecules are the principal scatterers of UV radiation and this lower air column

density above the Mauna Loa Observatory results in a much larger amount of UV-B radiation being transmitted to the instruments.

One of the objectives of this study was to compare the magnitudes of the ultraviolet and shortwave events. Table 3 provides the same maximum total shortwave events as cited in Table 2 but the ultraviolet MAC and PAC values were generated from the UV-A and UV-B CSIR events corresponding to the total shortwave events. From Table 3 it is evident that the magnitudes of the ultraviolet CSIR are somewhat variable for similar shortwave conditions. For example, total shortwave MAC and PAC values are almost identical for the days of July 3 and July 19; however, the UV-A PAC calculations on July 19 exhibited a 1.3% smaller magnitude but a 4.5% larger value in the UV-B. Also, the last three days in Table 3 show that no ultraviolet CSIR events were observed in conjunction with significant total shortwave events. Because not much was known about the actual cloud structure associated with these events, it is possible that cloud geometry may have influenced this variability in ultraviolet CSIR magnitudes. Also, ultraviolet radiation is very sensitive to atmospheric aerosol concentration and the UV-B, in particular, to ozone column amounts. These atmospheric variables are strongly affected by synoptic conditions and may change significantly during the day. Changes in these factors may manifest themselves as variations in the ultraviolet clear-sky curves. If the conditions during the actual CSIR day are slightly different than those which occurred in the compositing days, the clear-sky curve will underestimate or overestimate the actual clear-sky conditions. This will inherently affect the MAC and PAC calculations.

Segal and Davis (1990) suggested that CSIR events must have large durations in order to be climatologically significant. On average, the data from the Colorado sites exhibited CSIR durations of up to an hour with pronounced CSIR events lasting between 15 to 30 minutes. A major factor in these long durations was the orographically induced, non-random cloudiness occurring near the measurement sites. The duration of a CSIR event is a function of the sun-cloud-sensor geometry and the speed of cloud propagation. The CSIR events at West Lafayette were generally short lived but at all three wavelength ranges, CSIR durations of up to 30 minutes

were observed. While these durations are similar in magnitude to those reported by Segal and Davis (1990), the values of the mean PAC were smaller due to less favorable cloud conditions.

**5. Discussion**

The magnitudes of the CSIR events observed by the RARMF pyranometers proved to be significant during scattered cumulus cloud conditions. The main objective of this study was to quantitatively determine the relationship between shortwave and ultraviolet CSIR events. Theoretically, ultraviolet reflection should produce smaller CSIR at the surface due to the increased diffuse radiation impinging on the sides of clouds. The pyranometer data supported this conclusion with shortwave PAC magnitudes averaging 8.4% and 10.5% larger than the values calculated in the UV-A and UV-B regions respectively. However, the ultraviolet PAC magnitudes did not exhibit a consistent pattern relative to the shortwave magnitudes. As was discussed earlier, CSIR events of the same shortwave magnitude, occurring at the same time of day, corresponded to varying CSIR behavior in the UV-A and UV-B wavelengths. This is also evident in Table 2. Reasons for this behavior could be related to the sensitivity of ultraviolet radiation to the geometry of clouds or to the sensitivity of the generated clear-sky curve to changes in aerosol concentration and ozone column amounts.

The time durations of the RARMF CSIR events, while significant in magnitude, did not suggest major climatological implications. In Colorado, Segal and Davis (1992) encountered non-random cloudiness due to the orographic nature of the region. The significance of this type of cloudiness has two effects: increased duration of CSIR events and CSIR development at approximately the same time of day. While CSIR did occur at around noon for the seven days in this study, the durations were only half of those recorded in the Colorado study. Also, significant shadowing effects associated with the random nature of the scattered cumulus over West Lafayette further reduced the climatological impact of CSIR measured by RARMF pyranometers. Moreover, only seven days in the months of June, July and August were found to contain CSIR. Seasonal and possibly even monthly averages would smooth the effects caused by cloud reflectance. This indicates that under normal circumstances, the elevated levels of UV-A and

UV-B irradiance that occur under scattered cloud conditions may not be of concern. This assumes that it is the time integrated dose that is biologically significant. However, if peak doses are of concern, then CSIR events should probably be considered.

**Acknowledgements**

This study was supported by a Showalter Trust grant and NASA grant NAGW-3150. We wish to thank C.J. Fuqua and Robert Green for their assistance with the RARMF instrumentation and Professor John Snow for initiating the RARMF program.

**References**

Cahalan, R.F., W. Ridgway, W. Wiscombe, S. Gollmer, and Harshvardhan, 1994: Independent pixel and Monte Carlo estimates of stratocumulus albedo, *Journal of Atmospheric Sciences*, **51**, 3776-3790.

Cess, R.D., M.H. Zhang, P. Minnis, L. Corsetti, E.G. Dutton, B.W. Forgan, D.P. Garber, W.L. Gates, C.N. Long, J.-J Morcrette, G.L. Potter, V. Ramanathan, B. Subasilar, C.H. Whitlock, D.F. Young, and Y. Zhou, 1995: Absorption of solar radiation by clouds: Observations versus models. *Science*, **267**, 496-499.

Davies, R., 1978: The effect of finite geometry on the three-dimensional transfer of solar irradiance in clouds. *Journal of Atmospheric Sciences*, **35**, 1712-1725.

Frederick, J.E. and H.E. Snell, 1990: Tropospheric influence on solar ultraviolet radiation: The role of clouds. *Journal of Climate*, **3**, 373-381.

Harshvardhan and W.L. Thomas, 1984: Solar reflection from interacting and shadowing cloud elements. *Journal of Geophysical Research*, **89**, 7179-7185.

Hayasaka, T., N. Kikuchi, and M. Tanaka, 1995: Absorption of solar radiation by stratocumulus clouds: Aircraft measurements and theoretical calculations. *Journal of Applied Meteorology*, **34**, 1047-1055.

McKee, T.B. and S.K. Cox, 1974: Scattering of Visible Radiation by Finite Clouds. *Journal of Atmospheric Sciences*, **31**, 1885-1892.

Mims, F.M. and J.E. Frederick, 1994: Cumulus clouds and UV-B. *Nature*, **371**, 291.

Nack, W.L. and A.E.S. Green, 1974: Influence of clouds, haze, and smog on the middle ultraviolet reaching the ground. *Applied Optics*, **13**, 2405-2415.

Pilewskie, P., and F.P.J. Valero, 1995: Direct observations of excess solar absorption by clouds. *Science*, **267**, 1626, 1629.

Ramanathan, V., B. Subasilar, G.J. Zhang, W. Conant, R.D. Cess, J.T. Kiehl, H. Grassl, and L. Shi, 1995: Warm pool heat budget and shortwave cloud forcing: A missing physics?. *Science*, **267**, 499-503.

Segal, M. and J. Davis, 1992: The impact of deep cumulus reflection on the ground-level global irradiance. *Journal of Applied Meteorology*, **31**, 217-222.

Weaver, J.F. and M. Segal, 1988: Some aspects of nonrandom cloudiness in solar energy applications. *Solar Energy*, **41**, 49-54.

Weinman, J.A. and Harshvardhan, 1982: Solar reflection from a regular array of horizontally finite clouds. *Applied Optics*, **21**, 2940-2944.

Yankee Environmental Systems Inc., 1991: Operations Manual for UVA-1 Ultraviolet Pyranometer.

Yankee Environmental Systems Inc., 1991: Operations Manual for UVB-1 Ultraviolet Pyranometer.

Yankee Environmental Systems Inc., 1993: Technical Note 93-01. Improved Calibration of the UVB-1 Pyranometer.

Table 1. List of CSIR days (mm-dd-yy) and the days used to create their corresponding clear-sky curves.

| CSIR Days | Wavelength Ranges Available | Clear-Sky Composite Days |
|---|---|---|
| 07-03-95 | SW, UV-A, UV-B | 07-02-95, 07-08-95 |
| 07-17-95 | SW | 07-18-95, 07-19-95 |
| 07-18-95 | SW, UV-A, UV-B | 07-18-95, 07-19-95 |
| 07-19-95 | SW, UV-A, UV-B | 07-18-95, 07-19-95 |
| 07-30-95 | SW, UV-A, UV-B | 07-29-95, 07-30-95, 07-31-95 |
| 08-01-95 | SW, UV-A, UV-B | 07-29-95, 07-30-95, 07-31-95 |
| 08-15-95 | SW, UV-A, UV-B | 08-12-95, 08-13-95, 08-14-95 |

Table 2 Maximum MAC values with associated PAC magnitudes.

| | Shortwave | | UV-A | | UV-B | |
|---|---|---|---|---|---|---|
| CSIR Day | MAC ($Wm^{-2}$) | PAC (%) | MAC ($Wm^{-2}$) | PAC (%) | MAC ($Wm^{-2}$) | PAC (%) |
| 07-03-95 | 130.1 | 14.1 | 3.2 | 10.1 | 0.0 | 0.0 |
| 07-17-95 | 129.4 | 14.2 | missing | missing | missing | missing |
| 07-18-95 | 151.5 | 16.6 | 3.4 | 8.7 | 0.069 | 7.8 |
| 07-19-95 | 130.4 | 14.3 | 2.5 | 6.4 | 0.064 | 7.7 |
| 07-30-95 | 102.6 | 16.2 | 1.1 | 3.0 | 0.031 | 3.3 |
| 07-31-95 | 89.2 | 10.6 | 0.6 | 1.8 | 0.0 | 0.0 |
| 08-15-95 | 60.6 | 7.7 | 0.2 | 2.4 | 0.0 | 0.0 |

Table 3 Total shortwave and ultraviolet MAC and PAC values correpsonding to the maximum total shortwave CSIR event during each day.

| | Shortwave | | UV-A | | UV-B | |
|---|---|---|---|---|---|---|
| CSIR Day | MAC ($Wm^{-2}$) | PAC (%) | MAC ($Wm^{-2}$) | PAC (%) | MAC ($Wm^{-2}$) | PAC (%) |
| 07-03-95 | 130.1 | 14.1 | 2.9 | 7.5 | 0.0 | 0.0 |
| 07-17-95 | 129.4 | 14.2 | missing | missing | missing | missing |
| 07-18-95 | 151.5 | 16.6 | 2.4 | 6.1 | 0.069 | 7.8 |
| 07-19-95 | 130.4 | 14.3 | 2.4 | 6.2 | 0.04 | 4.5 |
| 07-30-95 | 102.6 | 16.2 | 0.0 | 0.0 | 0.0 | 0.0 |
| 07-31-95 | 89.2 | 10.6 | 0.0 | 0.0 | 0.0 | 0.0 |
| 08-15-95 | 60.6 | 7.7 | 0.0 | 0.0 | 0.0 | 0.0 |

**Figure Captions**

Figure 1. Composited clear-sky shortwave irradiance curve in $Wm^{-2}$ using pyranometer data from August 12-14, 1995.

Figure 2. Composited shortwave data from Figure 1 in $Wm^{-2}$ plotted versus the cosine of the solar zenith angle. The solid curve is a third degree polynomial best fit line for the composited data.

Figure 3. Comparison of composite and best-fit line clear-sky generation techniques for the data from August 12-14, 1995.

Figure 4. RARMF Vaisala laser ceilometer data from July 18, 1995 showing cloud base height.

Figure 5. Comparison of clear-sky and observed RARMF total shortwave irradiance in $Wm^{-2}$ for July 18,1995.

Figure 6. As in Figure 5 but for UV-A.

Figure 7. As in Figure 5 but for UV-B.

Figure 8. Total shortwave MAC ($Wm^{-2}$) and PAC (percentage) for July 18, 1995.

Figure 9. As in Figure 8 but for UV-A.

Figure 10. As in Figure 8 but for UV-B.

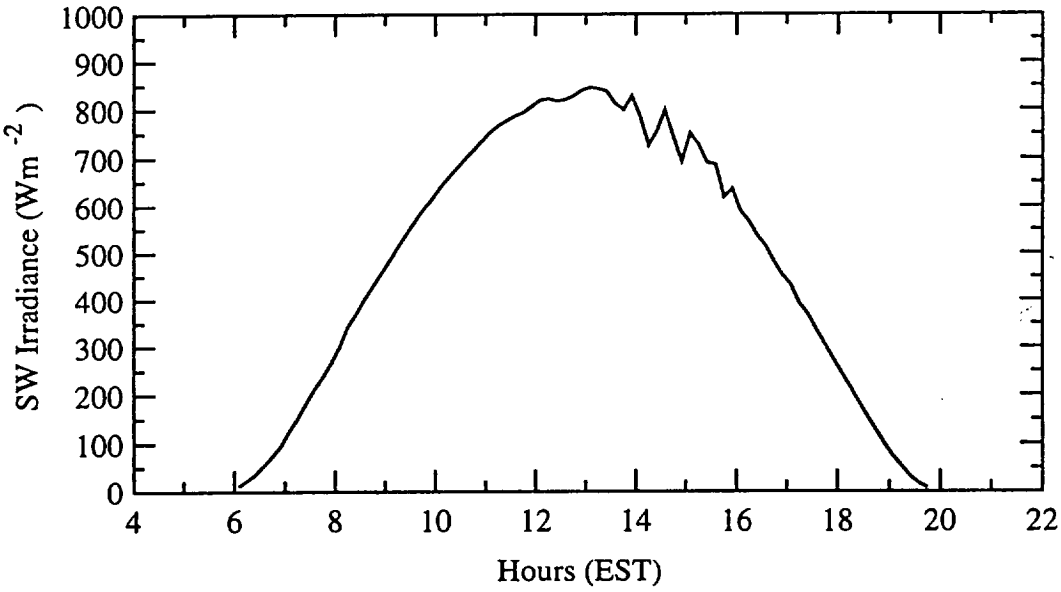
SW Irradiance (Wm -2 )
1000
900
800
700
600
500
400
300
200
100
0
4
6
8
10
12
14
16
18
20
22
Hours (EST)

Figure 1

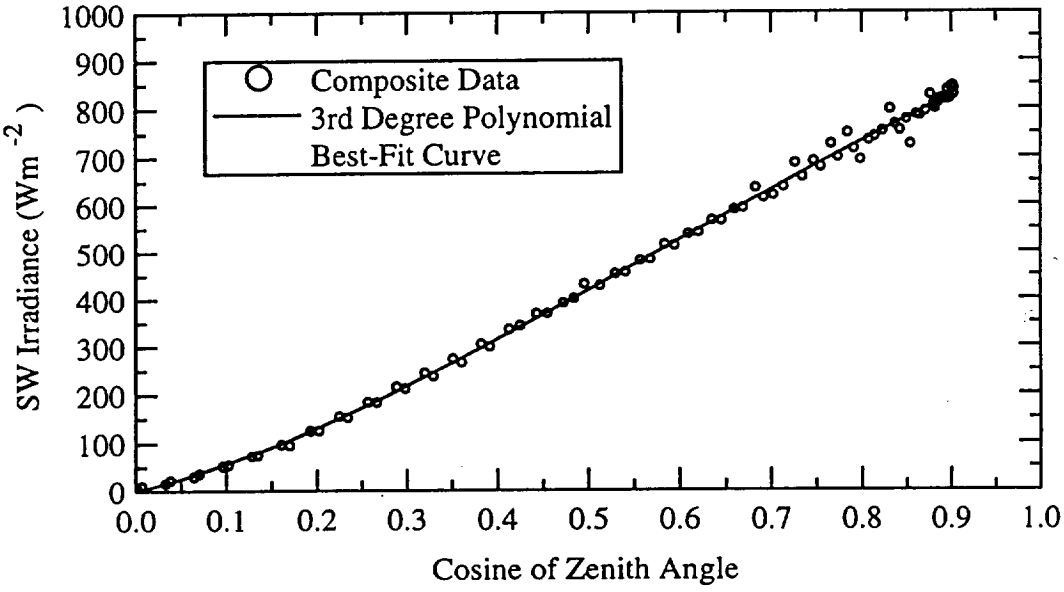
Composite Data
3rd Degree Polynomial
Best-Fit Curve
SW Irradiance (Wm -2 )
Cosine of Zenith Angle
0
100
200
300
400
500
600
700
800
900
1000
0.0
0.1
0.2
0.3
0.4
0.5
0.6
0.7
0.8
0.9
1.0

Figure 2

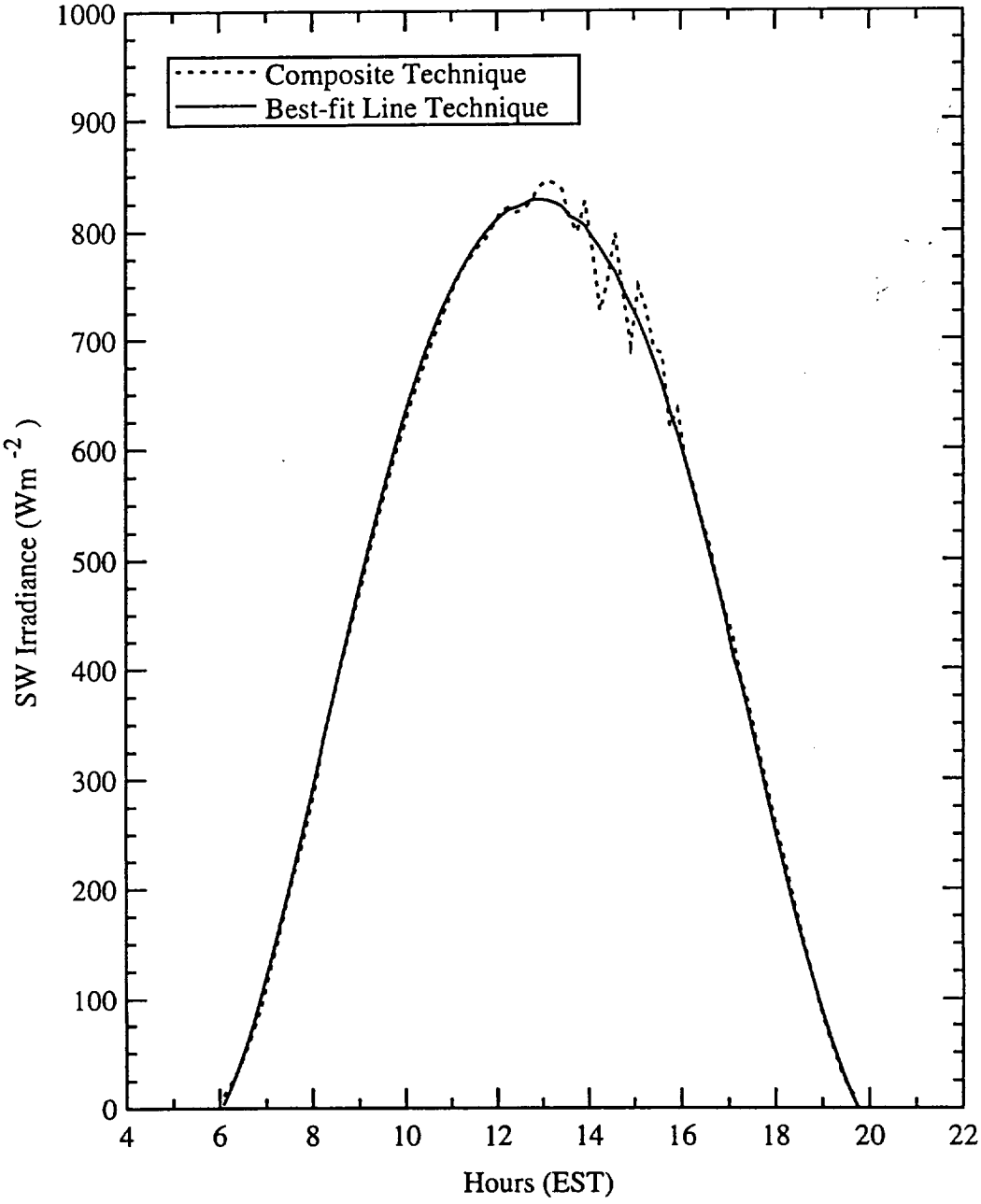
Composite Technique
Best-fit Line Technique
SW Irradiance (Wm -2 )
Hours (EST)
1000
900
800
700
600
500
400
300
200
100
0
4
6
8
10
12
14
16
18
20
22

Figure 3

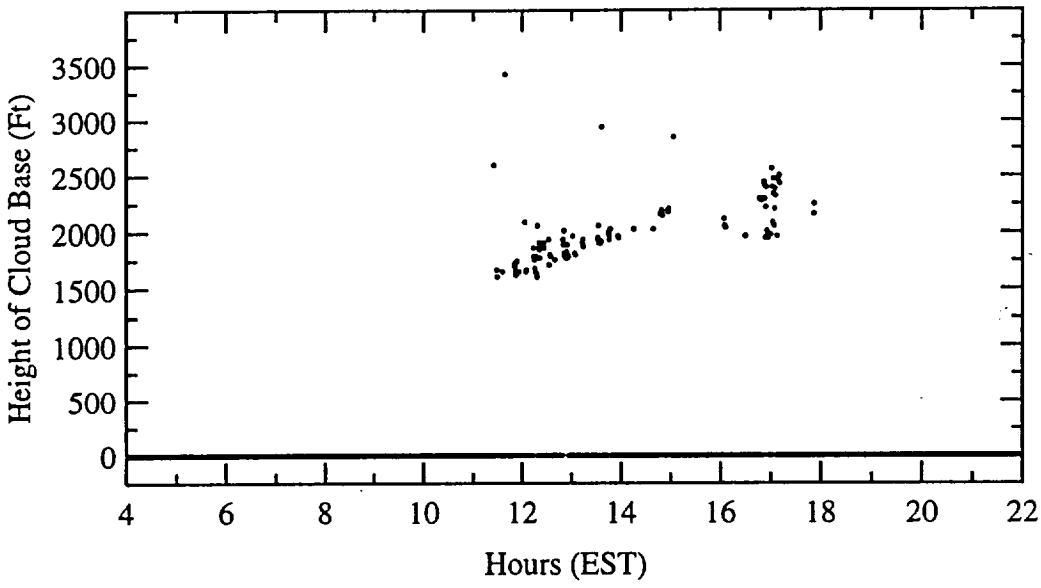
Height of Cloud Base (Ft)
3500
3000
2500
2000
1500
1000
500
0
4
6
8
10
12
14
16
18
20
22
Hours (EST)

Figure 4

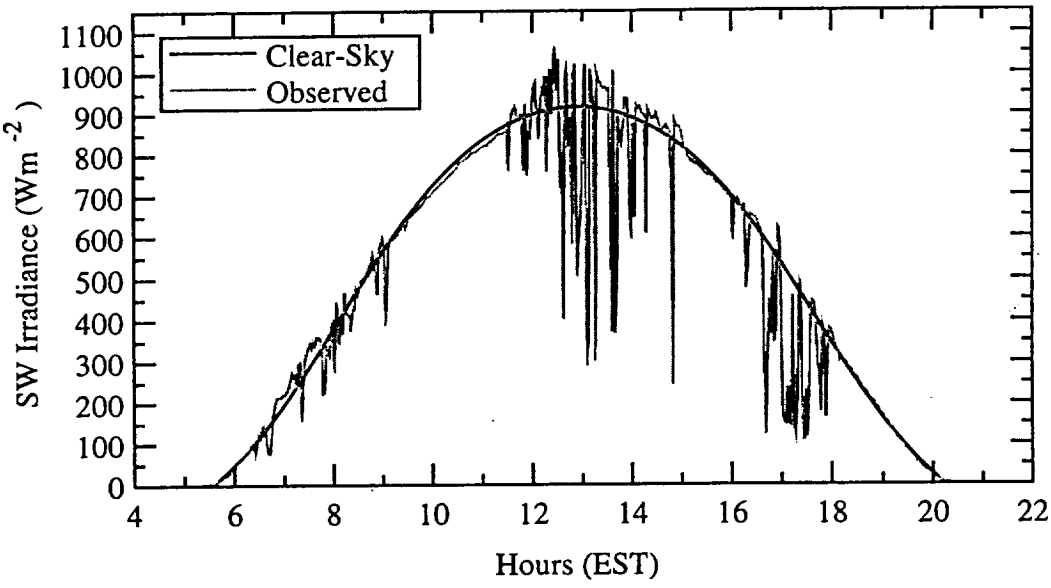
Clear-Sky
Observed
SW Irradiance (Wm -2 )
1100
1000
900
800
700
600
500
400
300
200
100
0
4
6
8
10
12
14
16
18
20
22
Hours (EST)

Figure 5

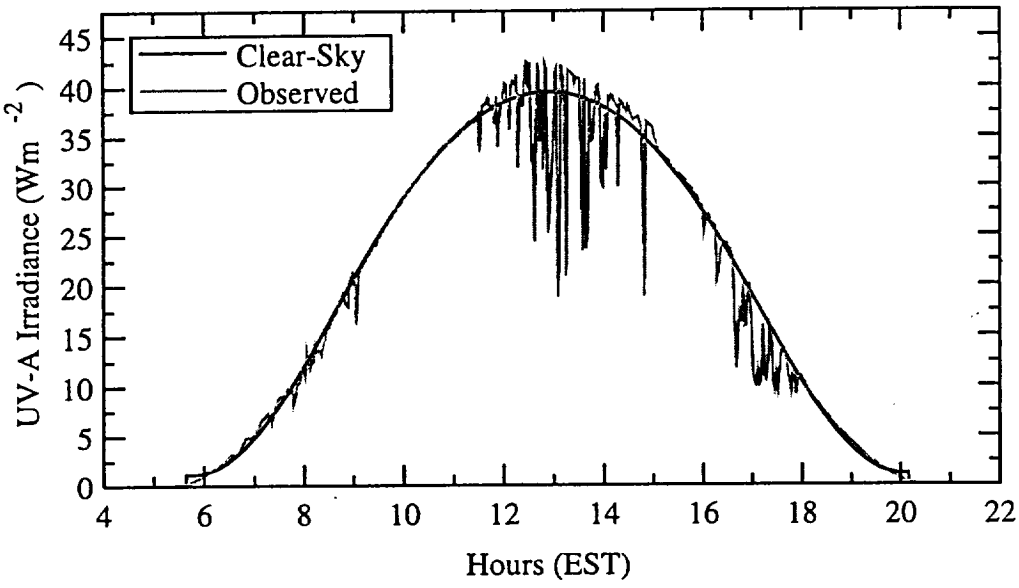
Clear-Sky
Observed
UV-A Irradiance (Wm -2 )
Hours (EST)
0
5
10
15
20
25
30
35
40
45
4
6
8
10
12
14
16
18
20
22

Figure 6

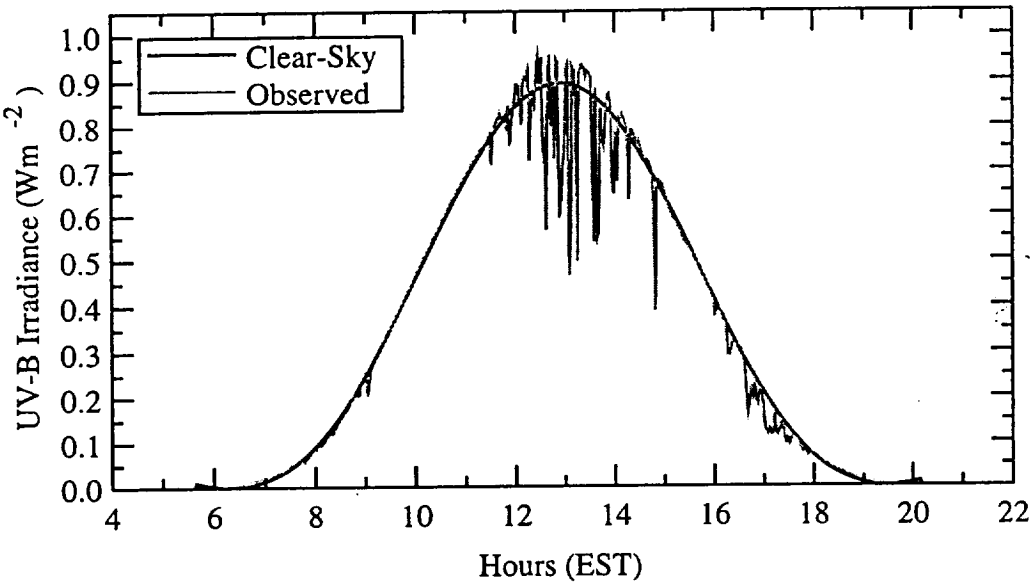
Clear-Sky
Observed
UV-B Irradiance (Wm -2 )
1.0
0.9
0.8
0.7
0.6
0.5
0.4
0.3
0.2
0.1
0.0
4
6
8
10
12
14
16
18
20
22
Hours (EST)

Figure 7

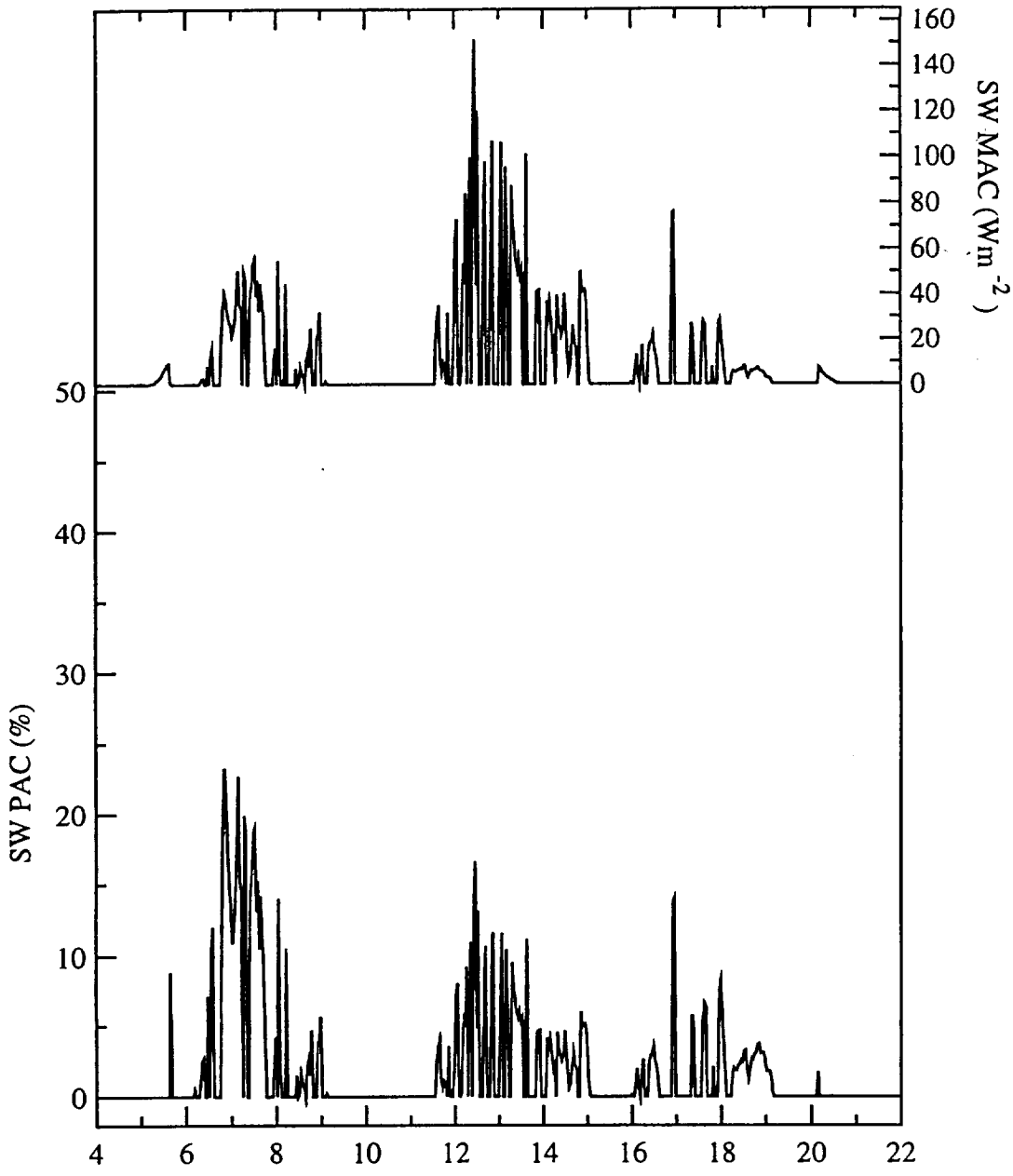
SW MAC (Wm$^{-2}$)
160
140
120
100
80
60
40
20
0
SW PAC (%)
50
40
30
20
10
0
4
6
8
10
12
14
16
18
20
22
Hours (EST)
Figure 8

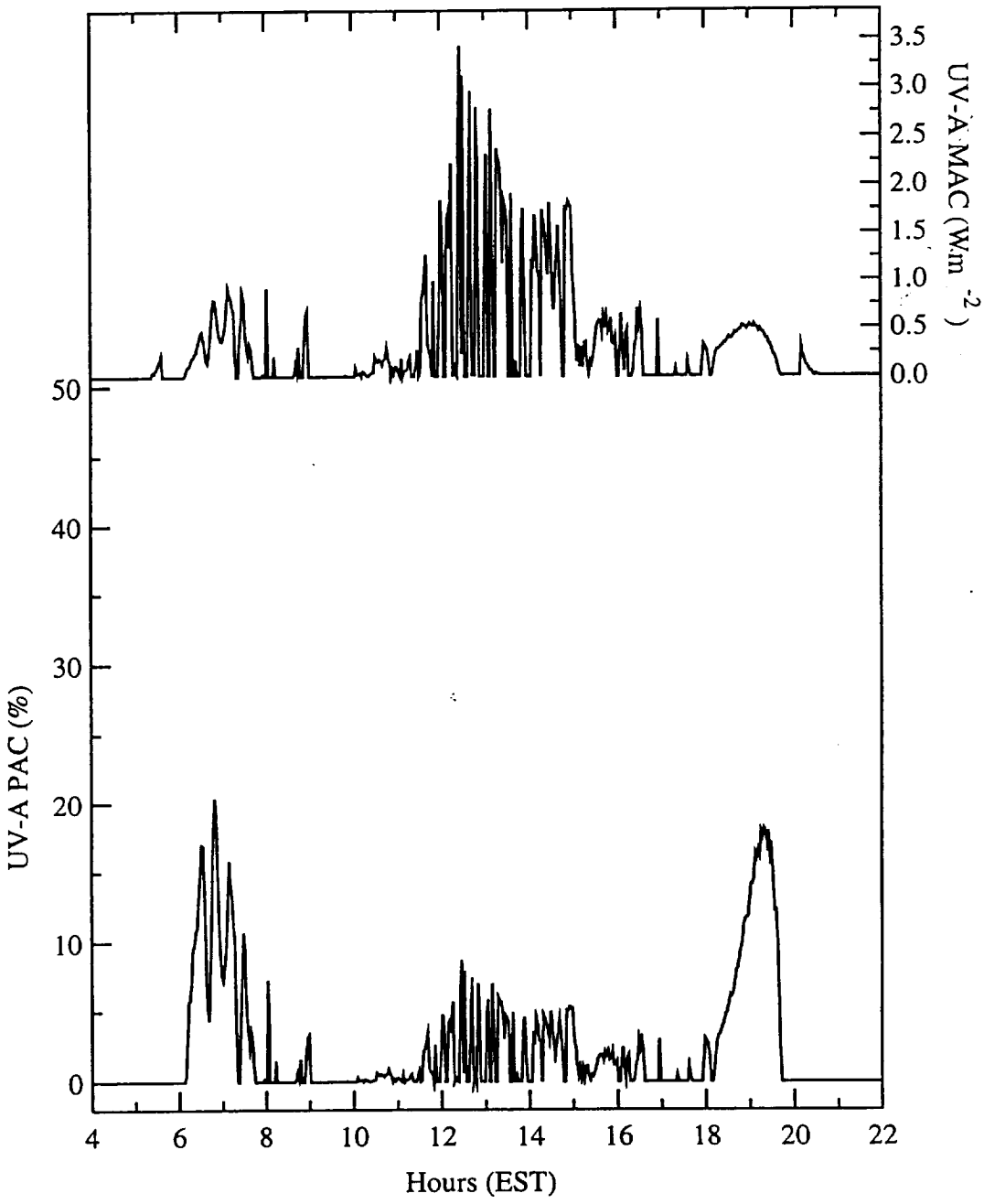
UV-A MAC (Wm -2 )
3.5
3.0
2.5
2.0
1.5
1.0
0.5
0.0
UV-A PAC (%)
50
40
30
20
10
0
4
6
8
10
12
14
16
18
20
22
Hours (EST)

Figure 9

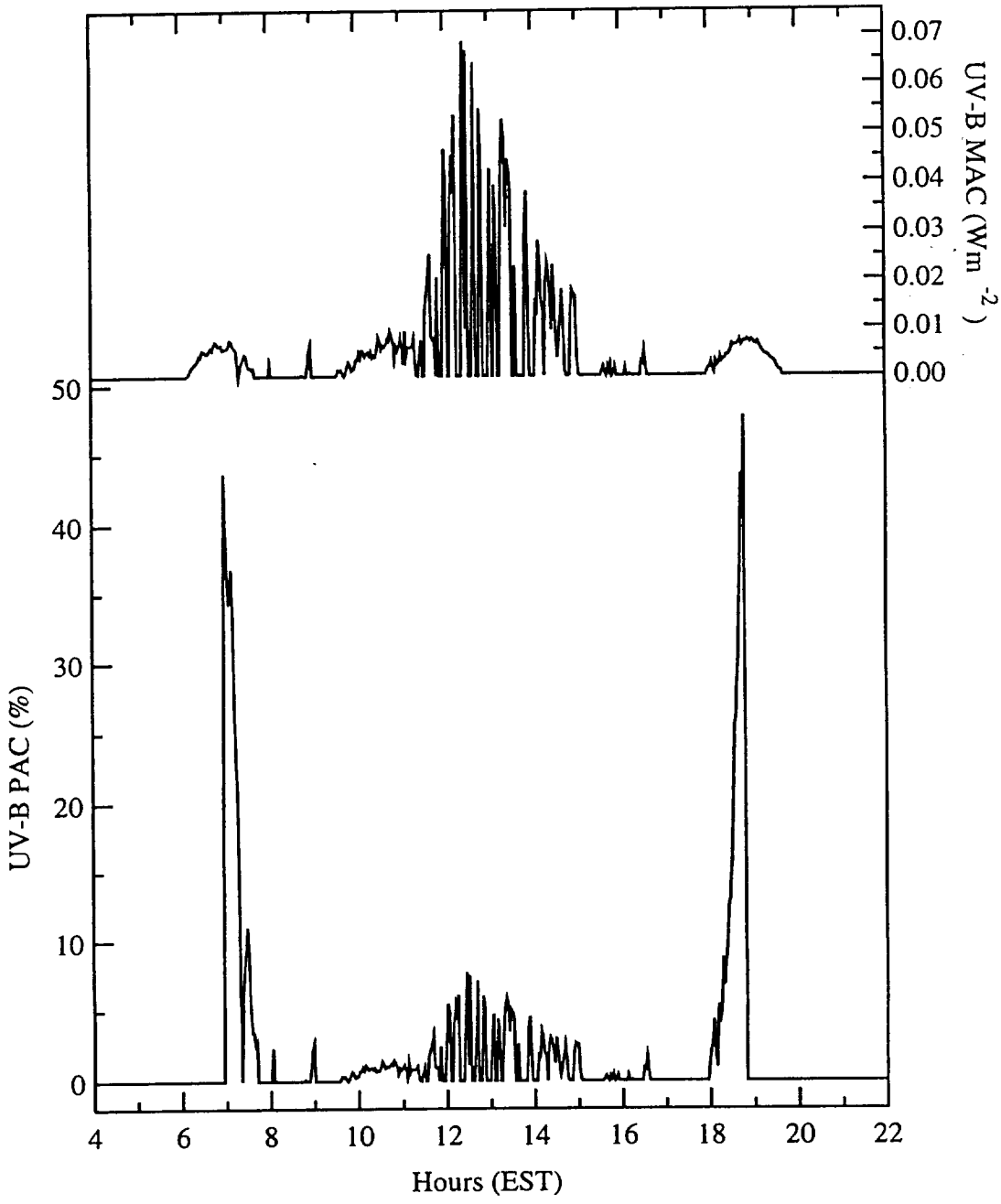
0.07
0.06
0.05
0.04
0.03
0.02
0.01
0.00
UV-B MAC (Wm -2 )
50
40
30
20
10
0
UV-B PAC (%)
4
6
8
10
12
14
16
18
20
22
Hours (EST)

Figure 10